Mirabito, C., D.N. Subramani, T. Lolla, P.J. Haley, Jr., A. Jain, P.F.J. Lermusiaux, C. Li, D.K.P. Yue, Y. Liu, F.S. Hover, N. Pulsone J. Edwards, K.E. Railey, and G. Shaw, 2017. Autonomy for Surface Ship Interception. In: Oceans '17 MTS/IEEE Aberdeen, 19-22 June 2017, DOI: 10.1109/OCEANSE.2017.8084817

Autonomy for Surface Ship Interception

C. Mirabito, D. N. Subramani, T. Lolla, P. J. Haley, Jr.,
A. Jain, P. F. J. Lermusiaux,
C. Li, D. K. P. Yue, Y. Liu, F. S. Hover
Department of Mechanical Engineering
Massachusetts Institute of Technology
77 Massachusetts Avenue
Cambridge, MA 02139
Email: pierrel@mit.edu

N. Pulsone, J. Edwards, K. E. Railey, G. Shaw
Lincoln Laboratory
Massachusetts Institute of Technology
244 Wood Street
Lexington, MA 02421-6426

***Abstract*—In recent years, the use of autonomous undersea vehicles (AUVs) for highly time-critical at-sea operations involving surface ships has received increased attention, magnifying the importance of optimal interception. Finding the optimal route to a moving target is a challenging procedure. In this work, we describe and apply our exact time-optimal path planning methodology and the corresponding software to such ship interception problems. A series of numerical ship interception experiments is completed in the southern littoral of Massachusetts, namely in Buzzards Bay and Vineyard Sound around the Elizabeth Islands and Martha's Vineyard. Ocean currents are estimated from a regional ocean modeling system. We show that complex coastal geometry, ship proximity, and tidal current phases all play key roles influencing the time-optimal vehicle behavior. Favorable or adverse currents can shift the optimal route from one island passage to another, and can even cause the AUV to remain nearly stationary until a favorable current develops. We also integrate the Kelvin wedge wake model into our path planning software, and show that considering wake effects significantly complicates the shape of the time-optimal paths, requiring AUVs to execute sequences of abrupt turns and tacking maneuvers, even in highly idealized scenarios. Such behavior is reminiscent of ocean animals swimming in wakes. In all cases, it is shown that our level set partial differential equations successfully guide the time-optimal vehicles through regions with the most favorable currents, avoiding regions with adverse effects, and accounting for the ship wakes when present.**

I. Introduction

The optimal interception of ships sailing on the ocean surface has numerous applications, including search and rescue operations, inspections of ship's hulls, ship repair and refueling, naval operations and planning, and management of underwater platforms. Interest in utilizing autonomous undersea vehicles (AUVs) for such applications has been increasing in recent years. In that case, the optimal recovery of these underwater vehicles by surface ships is also crucial. The time-sensitive nature of these operations render the search for an optimal route from a given point of deployment to a (possibly moving) target of paramount importance. However, numerous factors, including complex coastal geometry, time-varying and complicated currents, and a moving ship wake (further disrupting the local near-ship currents) make this a very challenging problem. Our present research motivation is thus to apply and extend our theory and schemes for optimal path planning of autonomous vehicles operating for long durations in strong and dynamic currents [1]–[4] to the optimal interception of surface vessels.

Our work focuses on exact time-optimal interception in dynamic ocean environments with multiple surface crafts and underwater vehicles. Previous results on related interceptions with AUVs are useful but they usually provide sub-optimal heuristic solutions or are restricted to specific aspects of the rendezvous problem; see, for example, [5]–[8]. For general reviews of autonomous underwater operations, we refer to [9]–[13].

The long-term goal is to develop autonomy for AUVs to enable intercept and proximity operations with underway surface vessels, predicting and optimally using dynamic wakes, surface waves, and underwater currents. After extending our time-optimal path planning to the ship interception problem, we study a set of simulated experiments for the Buzzards Bay, Vineyard Sound, and Elizabeth Islands region in Massachusetts. We combine realistic data-assimilative ocean modeling with rigorous time-optimal control and simple ship and wake modeling. To show the versatility of the autonomy approach and also illustrate how it is needed even for the simplest of the cases, we consider several different scenarios: environments with no flow at all but with several straits, cases with time-varying currents, and finally proximity operations considering the effects of ship wakes.

This paper is organized as follows. In sec. II, we briefly describe the underlying methodology of our time-optimal path planning software. Next, in sec. III, we apply this methodology to a variety of numerical experiments simulating the interception of either a stationary or moving ship, accounting for an ever-increasing number of effects, including complex coastlines, tidal currents, and ship wakes. Finally, some concluding remarks are made and possible future research directions are discussed in sec. IV.

II. Methodology

Our time-optimal path planning involves solving the fundamental Hamilton–Jacobi forward equation efficiently using

978-1-5090-5278-3/17/$31.00 ©2017 IEEE

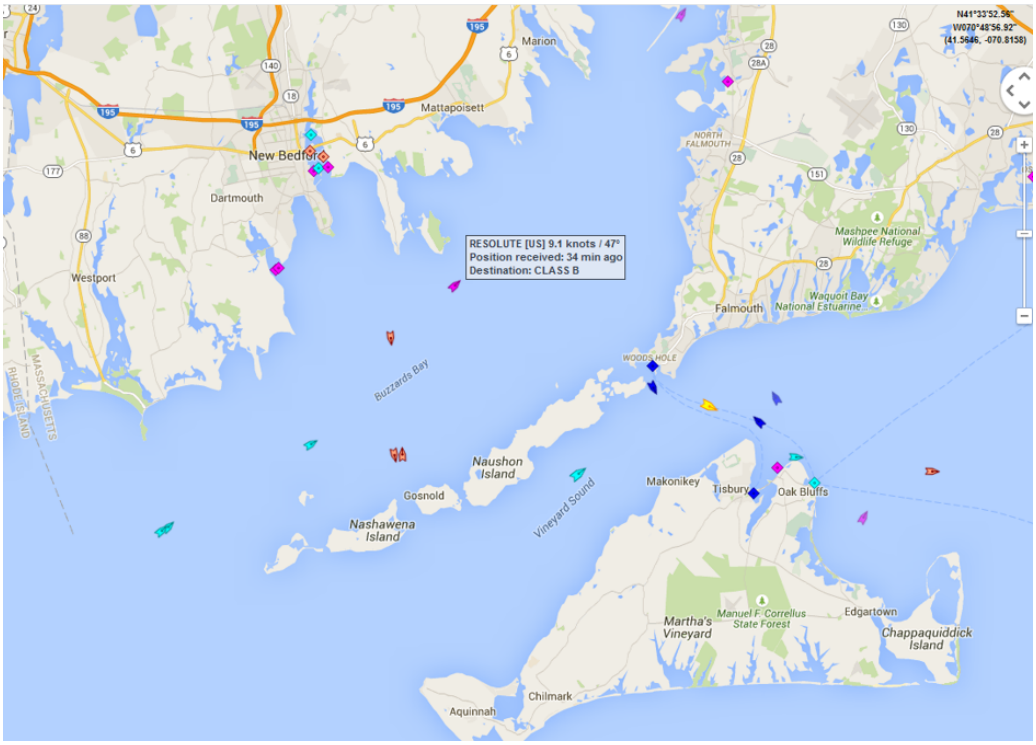

Fig. 1. Marine traffic in Buzzards Bay and Vineyard Sound, Massachusetts [14].

level set methods [2]:

$$\frac{\partial \phi(\mathbf{x},t)}{\partial t} + F|\nabla\phi(\mathbf{x},t)| + \mathbf{v}(\mathbf{x},t)\cdot\nabla\phi(\mathbf{x},t) = 0, \quad (1)$$

where t is time; F, the vehicle speed; $\mathbf{v}(\mathbf{x},t)$, the water velocity; and $\phi(\mathbf{x},t) = 0$, the level set of interest. That is, with an initial condition $\phi(\mathbf{x},0) = |\mathbf{x}-\mathbf{x}_0|$, the zero level set contour at time $t > 0$ is the reachability front of a vehicle starting at $\mathbf{x}_0$ at $t = 0$. The moving surface craft (i.e., the target) is modeled as

$$\frac{d\mathbf{x}_{Sh}(t)}{dt} = \mathbf{v}_{Sh}(t), \quad (2)$$

where $\mathbf{x}_{Sh}(t)$ is the ship's position at time t with starting point $\mathbf{x}_{Sh}(0)$ and where $\mathbf{v}_{Sh}(t)$ is the dynamic ship velocity. The target is first intercepted when the zero level set crosses its path at any given time. The optimal path is obtained by a backtracking algorithm [2]. A modified version of eq. (1) is solved when wakes are present; see sec. III-C.

III. Autonomy Experiments

Our numerical ship interception experiments take place in Buzzards Bay and Vineyard Sound, Massachusetts. These two bodies of water are separated by the Elizabeth Islands, a chain of small islands southwest of Woods Hole on Cape Cod, themselves separated by several narrow passageways, most notably Robinson's Hole (between Pasque and Naushon Island) and Quick's Hole (between Nashawena and Pasque Island); see fig. 1. The Sow and Pigs Reef marks the end of the island chain, and is located southwest of Cuttyhunk Island. In order to obtain realistic estimates of typical ship speeds and tracks in Buzzards Bay and Vineyard Sound, the web site MarineTraffic.com was used [14]; both small and large vessels typically travel with a speed of at most 10 kn.

The experiments discussed in this section are considered in order of increasing complexity. For example, when currents are considered ($\mathbf{v} \neq \mathbf{0}$), we obtain the current fields from the MSEAS-PE multiscale ocean modeling system [15], [16] forced with atmospheric forcing (from the National Centers for Environmental Prediction). Additionally, when ship wakes are present, wake models discussed in sec. III-C are used.

A. Effects of complex coastal geometry

1) Optimal routes without flow: We first consider the time-optimal interception under the effects of complex coastlines and of a moving target, a ship sailing at constant speed. The interception is to be made by a "fast" AUV but assuming $\mathbf{v} = \mathbf{0}$ (i.e., ignoring currents). As we will see, even in this seemingly simple case, due to multiply-connected geometry and the moving target, the time-optimal paths are far from obvious. For example, consider an AUV starting in Menemsha Bight, near Martha's Vineyard, attempting to intercept a ship located in Buzzards Bay and sailing southwest at a constant speed of 3 kn. The AUV's top speed F is 2 m/s (3.89 kn). Fig. 2 shows the level sets (i.e., reachability fronts) obtained and color-coded optimal routes to take when intercepting the ship, which depends on where the ship is at the time it is intercepted (the gray line indicates locations along the ship track where the ship cannot be intercepted 11,241 s after the

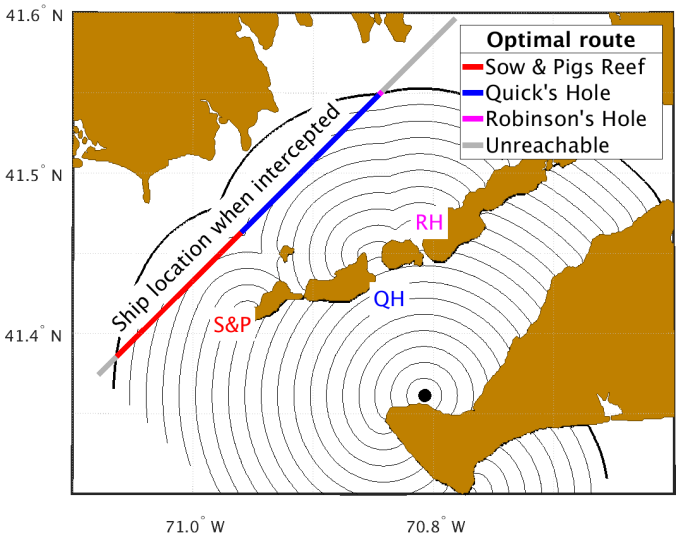

Fig. 2. Level sets and optimal routes for a single AUV intercepting a moving ship in Buzzards Bay.

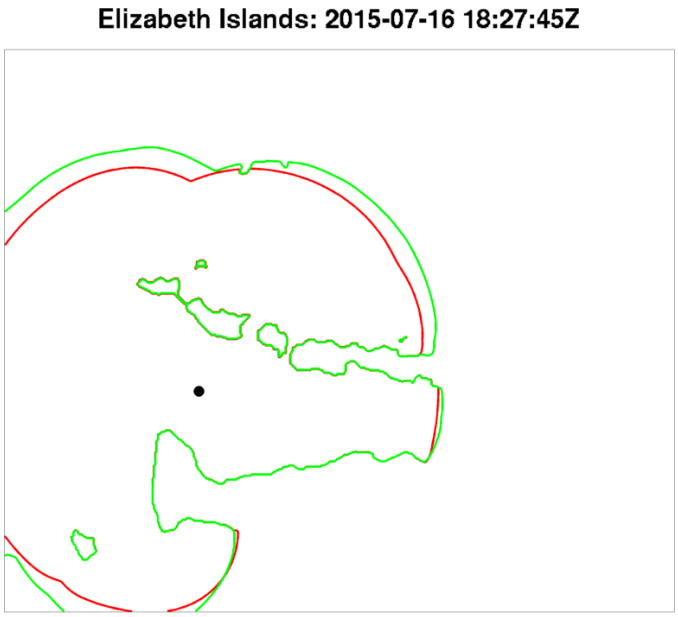

Fig. 3. Comparison of reachable points when $\mathbf{v} = \mathbf{0}$ (red) and $\mathbf{v} \neq \mathbf{0}$ (green) for a single AUV with a top speed of 2 m/s (3.89 kn) 9,756 s after deployment from Vineyard Sound.

AUV is deployed). The number of discontinuous shapes in the level sets is proportional to the number of islands; where these occur, there are at least two optimal routes from the starting point to the discontinuity locations, with the same arrival time. Since there are several passages between the islands, and hence several route choices, the optimal path to a moving target is far from straightforward to determine without our time-optimal level set method. Our results show that our efficient solution of the exact eq. (1) is needed. When $\mathbf{v} \neq \mathbf{0}$, guessing the fastest path becomes much more difficult and in general not feasible, even for AUVs that are fast compared to the currents.

2) Reachability Comparison: No flow versus ocean flow: The time-optimal paths can be strongly affected if tides and currents are considered ($\mathbf{v} \neq \mathbf{0}$), even for fast AUVs. To see this, consider again an AUV starting in Vineyard Sound with a top speed of 2 m/s (3.89 kn). The level sets (reachability fronts) 9,756 s after the AUV is deployed for $\mathbf{v} = \mathbf{0}$ (red) and $\mathbf{v} \neq \mathbf{0}$ (green) are shown in fig. 3. Four scenarios for ship interception are possible:

1) If the ship track is inside both the red and green level sets, the ship is reachable with or without flow.
2) If the ship track is inside the red level set but outside the green level set, the ship is no longer reachable when flow is considered.
3) If the ship track is outside the red level set but inside the green level set, flow effects must be considered in order to reach the ship.
4) If the ship track is outside both the red and green level sets, the ship cannot be intercepted after 9,756 s.

Note that reversing tidal currents can cause the with-flow reachability front to propagate at varying speeds (slower if an adverse current is present, faster if a favorable current is present), leading to the fronts overtaking each other at various stages of the tide (observed but not shown here).

B. *Effects of geometry and currents*

When $\mathbf{v} \neq \mathbf{0}$, the situation becomes more complicated, since differences between the maximum AUV speed F and current speed must be considered, in addition to differences between the maximum AUV speed and the ship velocity $\mathbf{v}_{Sh}(t)$: strong adverse currents can prevent a ship from being reachable within a given time, and, conversely, favorable currents can allow for an otherwise unreachable ship to be intercepted. As such, the choice of starting point (in addition to the ship's location and track) becomes important. To this end, we have developed accompanying software that searched for the starting points and (fixed) targets where the paths are most affected by the flow and coastline at the given deployment time, in terms of the time taken to reach the target point as well as the shape of the path; such computations serve as guidance on regions to avoid.

1) Slow vehicle and stationary target: We first consider a situation involving a slow AUV with a top speed F of 40 cm/s (0.78 kn) initially located in Vineyard Haven Harbor attempting to intercept a stationary target ($\mathbf{v}_{Sh}(t) = \mathbf{0}$) located in northern Vineyard Sound near Woods Hole, as shown in fig. 4a. At 2200Z on July 16, 2015, when the AUV is deployed, a strong adverse tidal current is present, with a speed far exceeding F. As a result, the AUV cannot traverse Vineyard Sound directly, since the current will push the vehicle eastward. Thus, the AUV must initially "wait" in Vineyard Haven Harbor (where the currents are weak), and then slowly travel along the coastline of northern Martha's Vineyard (where the current is adverse but weak) until a favorable current develops when the tide changes (this occurs at approximately 0100Z on July 17), at which time it crosses

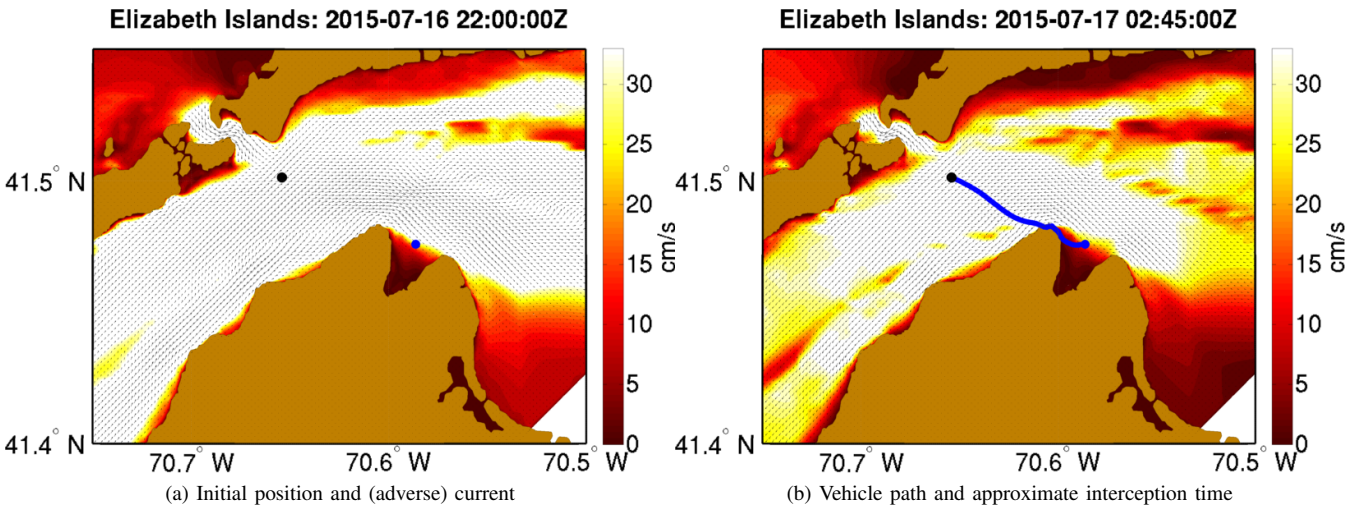

(a) Initial position and (adverse) current

(b) Vehicle path and approximate interception time

Fig. 4. Time-optimal path (blue) of an AUV deployed from Vineyard Haven Harbor intercepting a stationary target (black) located in northern Vineyard Sound. Paths are overlaid on instantaneous ocean currents (cm/s) at the snapshot time.

the sound and intercepts the target at approximately 0245Z on July 17; see fig. 4b. Overall, these results are consistent with the expected vehicle behavior of avoiding regions with strong adverse currents. This is directly accounted for by our methodology.

2) Vineyard Sound ship interception: In this example, we simulate four independent AUVs deployed along a line across the mouth of Vineyard Sound. Each vehicle is placed 5 km apart, and each has a maximum speed of 1 m/s (1.94 kn). All vehicles are attempting to intercept a ship initially located near Menemsha Bight and moving northeast at 1.15 kn (away from the AUVs). This area is subject to strong tidal currents, so the choice of starting time can play a crucial role in determining whether the ship can be intercepted. In this case, the starting time is 15:45Z on July 16, 2015, when the tidal current is moving toward the northeast (and hence is favorable for interception). Fig. 5 shows the resulting optimal paths taken by each vehicle; note that slight differences in the current profile perturb the paths, leading to small differences in arrival times.

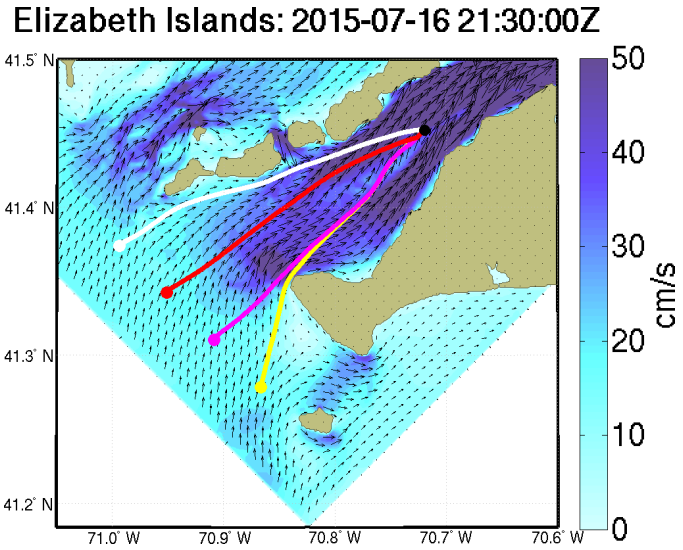

Fig. 5. Optimal paths for four independent AUVs intercepting a moving target (black) in Vineyard Sound. The ship is moving northeast at 1.15 kn; the maximum AUV engine speed is 1.94 kn. All AUVs are deployed on July 16, 2015 at 15:45Z. Paths are overlaid on instantaneous ocean currents (cm/s) at the snapshot time.

3) Buzzards Bay ship interception: We now simulate five independent AUVs deployed on July 16, 2015 at 1545Z along a line running northeast from the mouth of Vineyard Sound to the center of the Sound (between Martha's Vineyard and Naushon Island); see fig. 6. Each vehicle is again placed 5 km apart, and each has a top engine speed of 1 m/s (1.94 kn). The ship is initially located in the northeast corner of Buzzards Bay, and is moving southwest at 3 kn through the Buzzards Bay ship channel. Since the ship speed exceeds the vehicle speeds, the choice of starting point is significant; paths with starting points located farther northeast can fail to intercept the ship, especially in adverse currents. Also, unlike in the previous test case, the choice of route to cross into Buzzards Bay from Vineyard Sound is important: the AUVs have the choice of reaching Buzzards Bay by either rounding the tip of the Sow and Pigs Reef, or passing though either Quick's Hole or the narrower Robinson's Hole. Fig. 6 shows a snapshot of the current field, the time-optimal paths, and routes chosen, 4 hours after the missions begin. At the time shown, the missions are in progress; not all interceptions have yet been made. Notice that the three vehicles starting farthest into Vineyard Sound all cross into Buzzards Bay through Quick's Hole, and not Robinson's Hole (this crossing occurs at approximately 17:30Z), since the current is more favorable there during that time. The two remaining vehicles take advantage of the favorable current near the Sow and Pigs Reef.

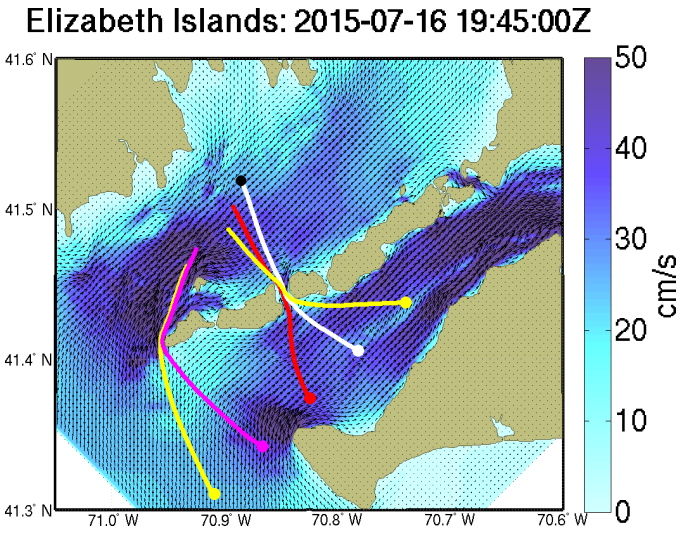

Fig. 6. Optimal paths for five independent AUVs deployed at July 16, 2015 at 15:45Z from Vineyard Sound intercepting a moving target (black) located in Buzzards Bay. The target is moving southwest at 3 kn; the maximum AUV engine speed F is 1 m/s (1.94 kn). Paths are overlaid on instantaneous ocean currents (cm/s) at the snapshot time of 19:45Z.

C. Ship wake modeling and prediction

The presence of wakes behind moving ships affects the local currents [17], [18], and hence the optimal path for the intercepting AUV. To account for this effect, an appropriate wake model must be chosen and implemented, modifying eq. (1) accordingly. Numerous ship wave and wake models have been developed in previous work; here, we only briefly review a few of them. For a more complete survey of ship motion models, see Lin and Kuang [19]. An early model was formulated by Lord Kelvin, where the ship is treated as a pressure point source in calm, deep water with a constant, subcritical velocity [20], [21]. The wake shape is formed by tracing the parametric equations

$$x = -\frac{a}{4}(5\cos\theta - \cos 3\theta), \tag{3}$$

$$y = -\frac{a}{4}(\sin\theta + \sin 3\theta), \tag{4}$$

where $\theta \in [-\frac{\pi}{2}, \frac{\pi}{2}]$ and $a > 0$ is constant (see fig. 7). For one ship, four regions are present, which are displayed in fig. 8: (i) the transverse wave region, where wave crests are approximated as orthogonal to the ship track; (ii) and (iii), the divergent wave regions on the port and starboard sides, respectively; and (iv), the region outside the wake, where the vehicle speed and flow profile are unaffected.

To integrate this wake model with the path planning software, the vehicle speed is described by a polar diagram inside each wake region (see fig. 9). For S ships, the modified level set equation (1) for $N = 3S + 1$ regions is

$$\frac{\partial\phi}{\partial t} + \sum_{i=1}^{N} F_i[\mathbf{x} \in R_i]|\nabla\phi| + \sum_{i=1}^{N} \mathbf{v}_i[\mathbf{x} \in R_i] \cdot \nabla\phi = 0, \tag{5}$$

where the vehicle speeds F_i depend on the angle relative to the ship track and the wave angle relative to AUV path (here

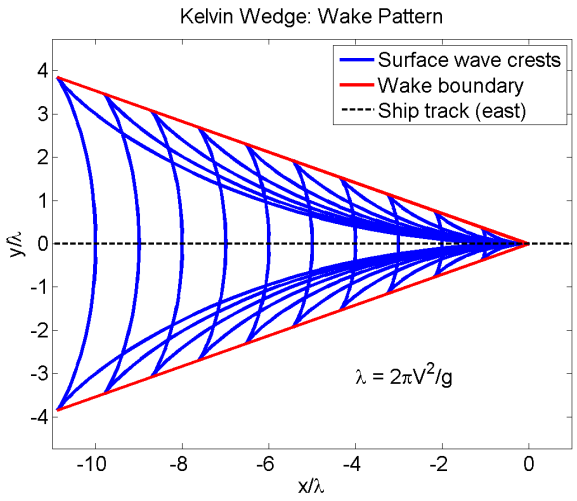

Fig. 7. The Kelvin wedge for a ship moving at velocity V in the x-direction.

assumed constant within each region), and the conditional $[\mathbf{x} \in R_i]$ is 1 if the point lies inside region R_i and zero otherwise.

Later, the Wigley hull model was developed [22], which accounts for the length of the ship, and is often used as benchmark in numerical simulations. The hull surface has an analytic form, and is defined by the expression

$$\frac{y}{B} = \left[1 - \left(\frac{2x}{L}\right)^2\right]\left[1 - \left(\frac{z}{D}\right)^2\right]\left[1 + 0.2\left(\frac{2x}{L}\right)^2\right], \tag{6}$$

where B denotes the ship's beam; L, its length, and D, its draft [23]. Other models in use include the thin-ship model [24], [25], the slender body model [26], models with a constant strength source and a moving pressure distribution [27], and the Taylor Series 60 hull [28]. More recently, nonlinear Reynolds-averaged Navier–Stokes (RANS) and turbulent models have been employed, based on potential flow methods [29]–[32], and have been applied to the study of solitons, monochromatic waves, depression areas, and supercritical bores [33], as well as decreasing wake angle as $1/|\mathbf{v}|$ for large ship speeds [34].

Recently, the Quadratic Boundary Element Method (QBEM) prediction tool, developed at the Vortical Flow Research Laboratory (VFRL) of MIT [35], has been developed and applied to the Wigley hull (see fig. 11). Based on the potential flow formulation and Mixed Eulerian Lagrangian method (MEL) for free surface and body position tracking, QBEM performs direct time-domain numerical simulation of wave-body interaction [36]. At each time step, the quadratic boundary element method is employed to solve the boundary integral equation of the boundary value problem for determining the normal velocity on the free surface and the velocity potential (and thus dynamic pressure) on the body surface. The fourth-order Runge–Kutta (RK4) scheme is then applied for time integration of the free surface boundary conditions and the equation of motion of the body for updating the positions of the free surface and body.

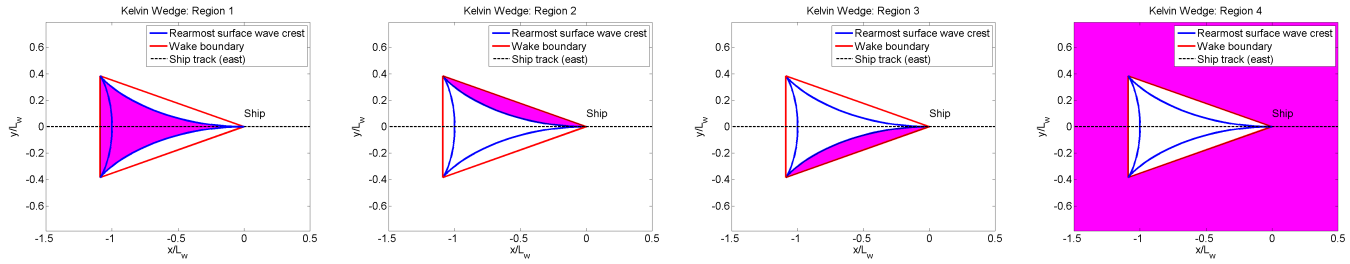

(a) Transverse wave region (interior) (b) Divergent wave region (port) (c) Divergent wave region (starboard) (d) Outside wake

Fig. 8. Regions of the Kelvin wedge.

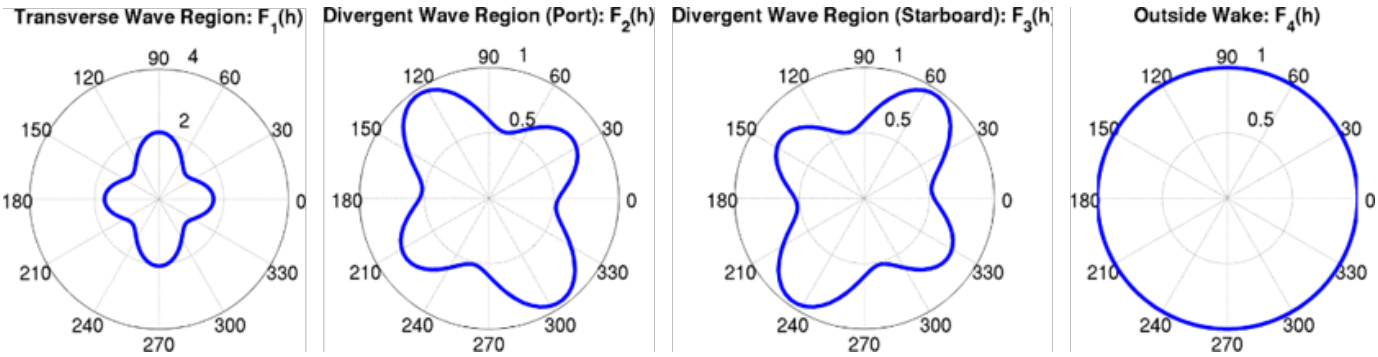

Fig. 9. Polar diagrams showing the vehicle speed F as a function of heading relative to the ship track for each region of the Kelvin wedge, using the base magnification.

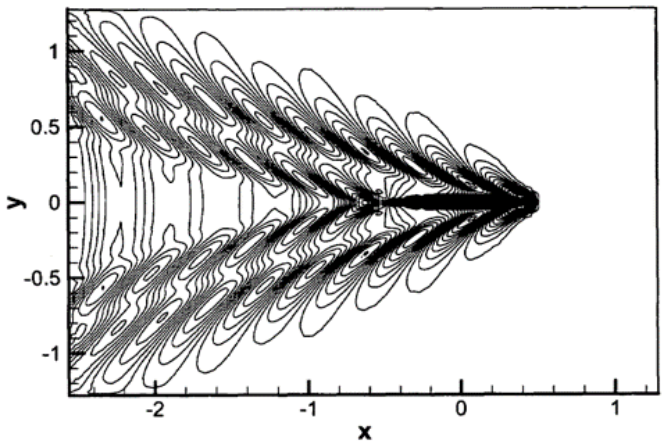

Fig. 10. Nonlinear wake solution from a pseudo-spectral model [19].

In the examples presented in the following sections, we first imagine a ship with exaggerated wake effects based on the Kelvin wedge.

1) Wake effects without flow: To get started, we will first show that even in idealized settings, and without considering the effects of currents, it remains difficult to predict the time-optimal path. This is mostly because the ship wakes can cause abrupt perturbations in the path.

a) Interception with a single ship and wake: To test the effect of the wake, we consider first a single AUV initially placed at $(0.1, 0.15)$ attempting to intercept a ship located at $(1, 0.75)$. The length of the wake L_w is set to 0.75, and the vehicle speed magnification factors are 1, $\frac{5}{7}$, $\frac{5}{7}$, and $\frac{3}{4}$ for F_1, F_2, F_3, and F_4, respectively (cf. fig. 9). Fig. 12 shows the intermediate level set contours and resulting time-optimal path. A consequence of our choice of magnification factors in this example is that it is advantageous for the AUV to travel inside the wake. The vehicle therefore enters the transverse wave region before making its final approach to the ship, employing a tacking maneuver in the process.

b) Multiple ships and tracks: We now consider the effects of having multiple ships present. In this case, a single AUV is initially placed at $(0.1, 0.1)$, and it attempts to intercept a ship located at $(0.9, 0.9)$. However, two other ships cross the region between the AUV's starting location and target ship. One of these ships is initially located at $(0, 0.75)$ and moves southeast ($\mathbf{v}_{Sh}(t) = (1, -1)$); the second ship starts at $(1, 0.25)$ and moves northwest ($\mathbf{v}_{Sh}(t) = (-0.5, 0.5)$). The wake length $L_w = 0.3$ for all three ships. When two or more wakes interact, the effect is assumed to be additive. The vehicle speed magnification factors are 1, 1, 1, and 0.5 for F_1, F_2, F_3, and F_4, respectively, for all ships, again rendering it advantageous for the vehicle to travel inside the wakes. Fig. 13 shows the level sets and time-optimal path. The path interacts with the wakes of both crossing ships, as well as the target ship, requiring the AUV to turn abruptly as it passes from one wake region to another.

c) Interception and avoidance of a ship convoy: Continuing the theme of multiple ships and tracks, we consider

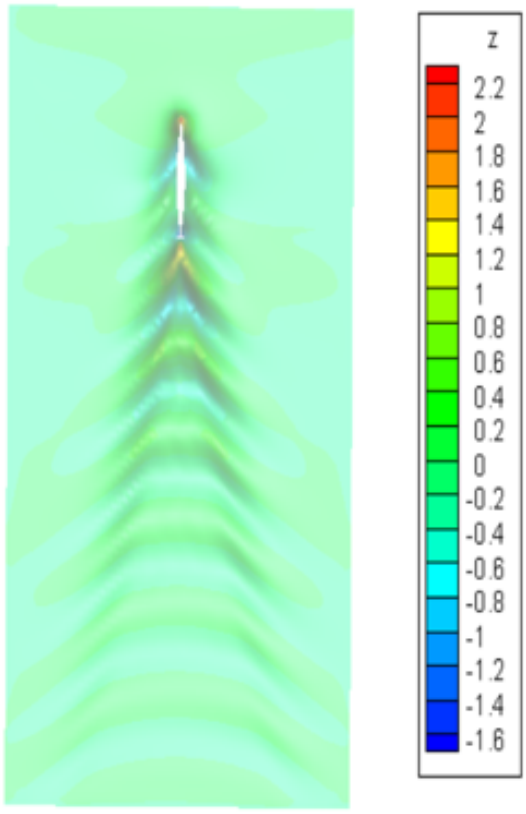

Fig. 11. QBEM solution for the free surface displacement (m) generated by a ship traveling at 10 m/s with a Wigley hull and $L = 100$ m, $B = 10$ m, and $D = 16$ m.

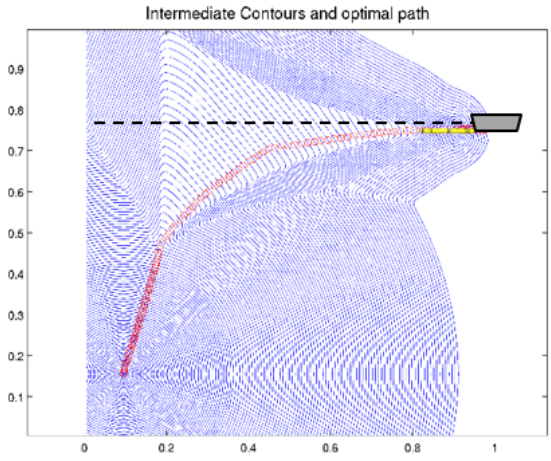

Fig. 12. Zero level sets (blue) and time-optimal path (red) for a single AUV intercepting and engaging a single ship with a wake.

in this example a single AUV initially located at $(0.5, 0.05)$ that attempts to reach a target point located at $(0.5, 0.95)$. A convoy consisting of five ships moving westward at unit speed, arranged such that there are two leading ships, one ship in the center, and two trailing ships, passes between the AUV and

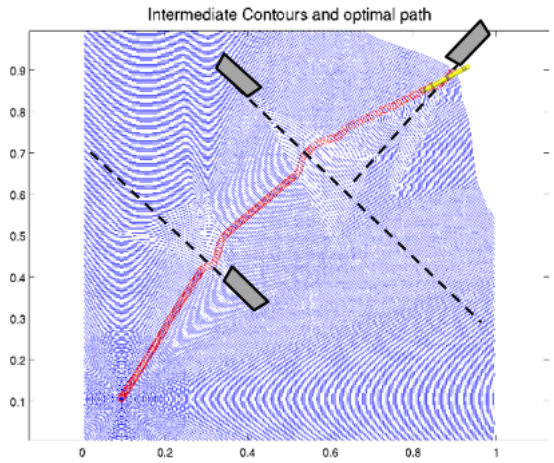

Fig. 13. Zero level sets (blue), time-optimal path (red), and ship tracks (black dashed lines) for a single AUV intercepting the ship located at $(0.9, 0.9)$.

the target; see fig. 14. The presence of the convoy makes it difficult for the AUV to avoid passing through the wakes on its way toward its target. The wake length $L_w = 0.5$ for all ships. The vehicle speed magnification factors are 1, 1, 1, and 0.75 for F_1, F_2, F_3, and F_4, respectively, for all ships, retaining the advantage for the vehicle to travel inside the wakes, but less than in the previous example. Consequently, a vehicle utilizing the time-optimal path to the target shown in fig. 14 heads directly into the approaching convoy, and then executes a long series of turns as it passes in and out of wakes and between wake regions. When the target is reached, the convoy has passed.

2) Wake and current effects: Lastly, we consider interception and engagement of multiple ships with wakes in an idealized setting that mimics the coastal geometry of the Elizabeth Islands. Eight independent AUVs are deployed, in two groups: One group of three AUVs, each placed 1 km apart (except for the top AUV, which is 2 km away from the middle AUV; see fig. 15), starts in Buzzards Bay near an idealized Cuttyhunk Island and behind Penikese Island, while the other group of five AUVs, again placed 1 km apart, starts in Vineyard Sound on the opposite side of Cuttyhunk Island. The targets are two ships located in Buzzards Bay, which are moving left to right with a constant speed of 1 kn. The lead ship is initially located at $(16, 10.5)$, while the trailing ship is 4 km behind the lead ship. Each group of AUVs attempts to intercept a different moving ship: the three AUVs in Buzzards Bay attempt to intercept the leading ship, while the five AUVs starting in Vineyard Sound attempt to intercept the trailing ship. Each ship has a wake length of 1 km. The maximum vehicle speed is approximately 1.62 kn outside the wake for all vehicles. The velocity field in this example is generated from finite volume software developed in the MSEAS group [37], assuming inflow from the left boundary and taking $\mathrm{Re} = 400$ in order to generate some turbulent effects.

Fig. 15 shows the time-optimal paths for each vehicle. Note

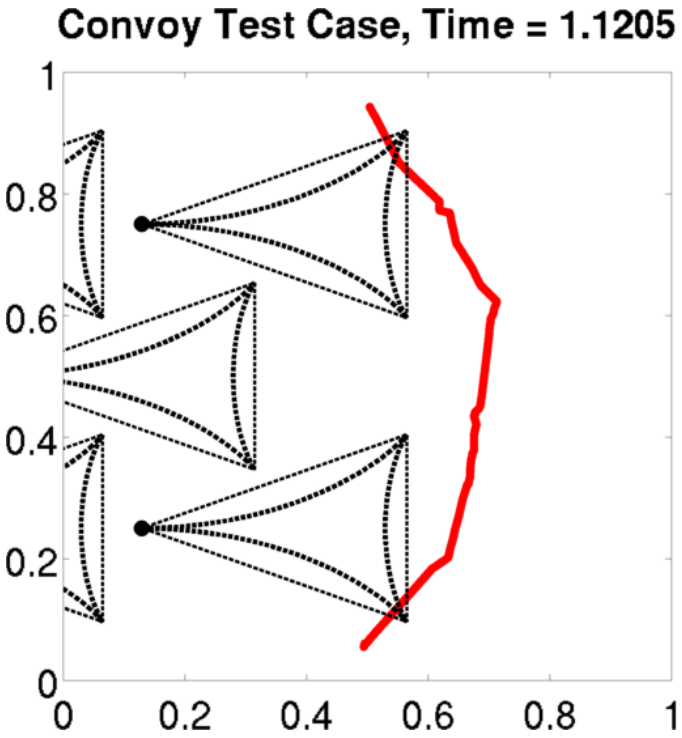

Fig. 14. Time-optimal path (red) taken by an AUV attempting to each a target located on the opposite end of the domain by passing through wake regions of ships in a passing convoy (black dashed lines). The convoy is moving from right to left at a constant speed.

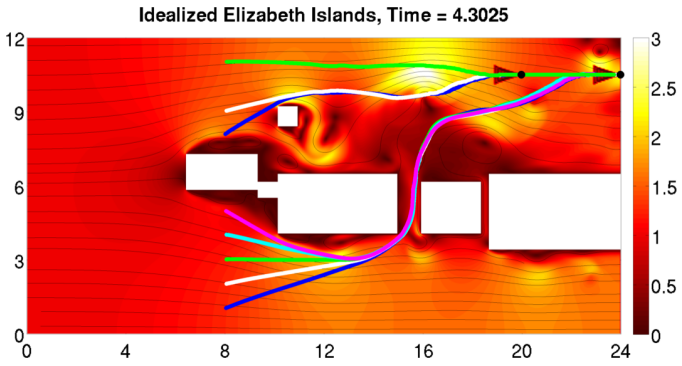

Fig. 15. Time-optimal paths of two groups of AUVs intercepting separate moving ships (black) in an idealized Elizabeth Islands domain. Paths are overlaid on instantaneous ocean current magnitude (km/h) and streamlines at the given snapshot time (hr).

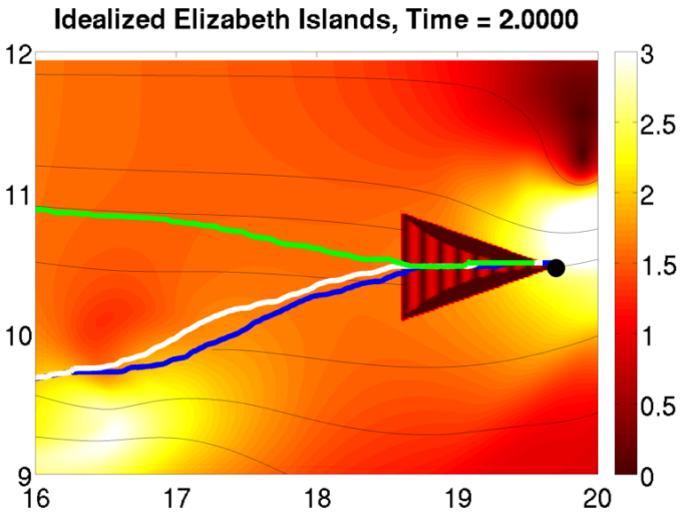

Fig. 16. Zoom on the engagement of the first intercepting AUV group (initially located in Buzzards Bay) with the lead ship wake. Paths are overlaid on instantaneous ocean current magnitude (km/h) and streamlines at the given snapshot time (hr).

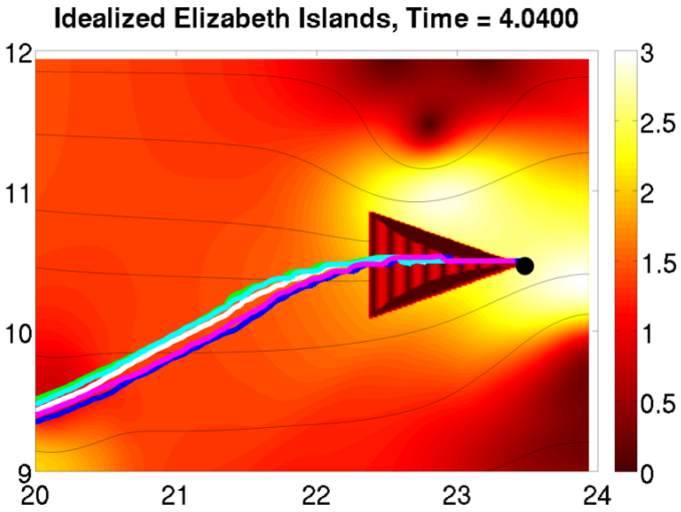

Fig. 17. Zoom on the engagement of the second intercepting AUV group (initially located in Vineyard Sound) with the trailing ship wake. Paths are overlaid on instantaneous ocean current magnitude (km/h) and streamlines at the given snapshot time (hr).

that the leading ship is intercepted first, and these vehicles are assumed to be collected by the ship once it is reached, and the missions are complete. The paths for the AUVs are then shown as the same as the ship track. Figs. 16 and 17 show zooms of the final approach of each group of vehicles to their respective targets. Each vehicle approaches its target ship through the central wake region, tacking slightly, similar to a sailboat encountering headwinds.

IV. Conclusion

We extended our time-optimal path planning to the dynamic interceptions of ships by a single AUV or groups of AUVs in multiply-connected regions with complex geometries and dynamic environments. Specifically, we illustrated results for diverse scenarios in the southern littoral of Massachusetts for varied ship and AUV speeds, start locations, and behaviors, with and without currents, and with and without ship wake effects. We combined realistic data-assimilative ocean modeling with rigorous time-optimal control and simple ship and wake modeling.

Multiple extensions of the present time-optimal interception results are possible. The present applications are connected to and can be combined with pursuit-evasion games and related game-theoretic ideas [38], [39] or networked control schemes for dynamic pursuits [40], [41]. They can also be extended to

time-optimal interceptions respecting specific pattern formations [42]. Other optimality criteria can also be utilized for the interception, such as energy-optimality [43]–[45]. More complex dynamic modeling of wakes and currents can also be included. Finally, based on recent results at sea with real AUVs [46], [47], utilizing the present schemes in real-time and with real vehicles and surface craft appears very promising for a wide range of critical applications.

ACKNOWLEDGMENT

We thank the members of our MSEAS group for useful discussions. We are grateful for the research support and guidance from the Technology and Contracts Office at MIT Lincoln Laboratory. We are grateful to the Office of Naval Research (ONR) for research support under grants N00014-14-1-0476 (Science of Autonomy - LEARNS) to the Massachusetts Institute of Technology (MIT). We also thank the MIT-Tata Center Program for the Fellowship support of DNS.

REFERENCES

[1] P. F. J. Lermusiaux, T. Lolla, P. J. Haley, Jr., K. Yigit, M. P. Ueckermann, T. Sondergaard, and W. G. Leslie, "Science of autonomy: Time-optimal path planning and adaptive sampling for swarms of ocean vehicles," in *Springer Handbook of Ocean Engineering: Autonomous Ocean Vehicles, Subsystems and Control*, T. Curtin, Ed. Springer, 2016, ch. 21, pp. 481–498.

[2] T. Lolla, M. P. Ueckermann, K. Yiğit, P. J. Haley, Jr., and P. F. J. Lermusiaux, "Path planning in time dependent flow fields using level set methods," in *IEEE International Conference on Robotics and Automation (ICRA), 14-18 May 2012*, 2012, pp. 166–173.

[3] T. Lolla, P. J. Haley, Jr., and P. F. J. Lermusiaux, "Time-optimal path planning in dynamic flows using level set equations: Realistic applications," *Ocean Dynamics*, vol. 64, no. 10, pp. 1399–1417, 2014.

[4] T. Lolla, P. F. J. Lermusiaux, M. P. Ueckermann, and P. J. Haley, Jr., "Time-optimal path planning in dynamic flows using level set equations: Theory and schemes," *Ocean Dynamics*, vol. 64, no. 10, pp. 1373–1397, 2014.

[5] S. M. Ahmad, R. Sutton, and R. S. Burns, "Retrieval of an autonomous underwater vehicle: An interception approach," *Journal of the Society for Underwater Technology*, vol. 25, no. 4, pp. 185–197, Dec. 2003.

[6] J. W. Nicholson, "Autonomous optimal rendezvous of underwater vehicles," Ph.D. dissertation, Naval Postgraduate School, Monterey, CA, Sep. 2004.

[7] C. Prévost, O. Thériault, A. Desbiens, É. Poulin, and E. Gagnon, "Receding horizon model-based predictive control for dynamic target tracking: a comparative study," in *AIAA Guidance, Navigation, and Control Conference*, Chicago, Aug. 2009.

[8] O. A. Yakimenko, D. P. Horner, and D. G. Pratt, "AUV rendezvous trajectories generation for underwater recovery," in *2008 16th Mediterranean Conference on Control and Automation*. IEEE, Jun. 2008, pp. 1192–1197.

[9] T. Schneider, H. Schmidt, T. Pastore, and M. Benjamin, "Cooperative autonomy for contact investigation," in *OCEANS 2010 IEEE - Sydney*. IEEE, May 2010, pp. 1–7.

[10] T. B. Curtin, J. G. Bellingham, J. Catipovic, and D. Webb, "Autonomous oceanographic sampling networks," *Oceanography*, vol. 6, no. 3, pp. 86–94, 1993.

[11] M. R. Benjamin, H. Schmidt, P. M. Newman, and J. J. Leonard, "Nested autonomy for unmanned marine vehicles with MOOS-IvP," *Journal of Field Robotics*, vol. 27, no. 6, pp. 834–875, Oct. 2010.

[12] A. Bahr, J. J. Leonard, and M. F. Fallon, "Cooperative localization for autonomous underwater vehicles," *International Journal of Robotics Research*, vol. 28, no. 6, pp. 714–728, Jun. 2009.

[13] F. S. Hover, R. M. Eustice, A. Kim, B. Englot, H. Johannsson, M. Kaess, and J. J. Leonard, "Advanced perception, navigation and planning for autonomous in-water ship hull inspection," *International Journal of Robotics Research*, vol. 31, no. 12, pp. 1445–1464, Nov. 2012.

[14] MarineTraffic, Apr. 2017. [Online]. Available: http://www.marinetraffic.com

[15] P. J. Haley, Jr. and P. F. J. Lermusiaux, "Multiscale two-way embedding schemes for free-surface primitive equations in the "Multidisciplinary Simulation, Estimation and Assimilation System"," *Ocean Dynamics*, vol. 60, no. 6, pp. 1497–1537, Dec. 2010.

[16] P. J. Haley, Jr., A. Agarwal, and P. F. J. Lermusiaux, "Optimizing velocities and transports for complex coastal regions and archipelagos," *Ocean Modeling*, vol. 89, pp. 1–28, 2015.

[17] H. Yan and Y. Liu, "An efficient high-order boundary element method for nonlinear wave–wave and wave-body interactions," *Journal of Computational Physics*, vol. 230, no. 2, pp. 402–424, Jan. 2011.

[18] Q. Zhu, Y. Liu, and D. K. P. Yue, "Resonant interaction of Kelvin ship waves and ambient waves," *Journal of Fluid Mechanics*, vol. 597, pp. 171–197, Feb. 2008.

[19] R.-Q. Lin and W. Kuang, "Numerical modeling of nonlinear ship-wave interactions," Jun. 2010, US Patent 7,734,449.

[20] W. Thomson, "On ship waves," in *Proceedings of the Institution of Mechanical Engineers*. London: Institution of Mechanical Engineers, Aug. 1887, pp. 409–433.

[21] H. Lamb, *Hydrodynamics*. New York: Dover, Apr. 1932.

[22] W. C. S. Wigley, "A comparison of experiment and calculated wave-profiles and wave-resistances for a form having parabolic waterlines," *Proceedings of the Royal Society A*, vol. 144, no. 851, pp. 144–159, Mar. 1934.

[23] J. M. J. Journée, "Experiments and calculations on 4 Wigley hull forms in head waves," TU Delft, Delft, Netherlands, Tech. Rep. 0909, May 1992.

[24] J. H. Michell, "The wave-resistance of a ship," *Philosophical Magazine Series 5*, vol. 45, no. 272, pp. 106–123, 1898.

[25] T. H. Havelock, "The propagation of groups of waves in dispersive media, with application to waves on water produced by a traveling disturbance," *Proceedings of the Royal Society A*, vol. 81, no. 549, pp. 398–430, Dec. 1908.

[26] E. O. Tuck, "A systematic asumptotic expansion procedure for slender ships," *Journal of Ship Research*, vol. 8, no. 1, pp. 15–23, 1964.

[27] J. V. Wehausen and E. V. Laitone, "Surface waves," in *Fluid Dynamics*, ser. Mechanical and Thermal Behaviour of Matter, C. A. Truesdell, Ed. Berlin: Springer, 1960, vol. 9, pp. 446–778.

[28] F. H. Todd, "Series 60 - Methodical experiments with models of single-screw merchant ships," David Taylor Model Basin, Washington, DC, Research and Development Report 1712, Jul. 1963. [Online]. Available: http://www.dtic.mil/dtic/tr/fulltext/u2/419990.pdf

[29] H. C. Raven, "A solution method for the nonlinear ship wave resistance problem," Ph.D. dissertation, TU Delft, Delft, Netherlands, Jun. 1996.

[30] ——, "Inviscid calculations of ship wave making—capabilities, limitations, and prospects," in *Proceedings of the 22nd Symposium on Naval Hydrodynamics*. Washington, DC: National Academy Press, 1998, pp. 738–754.

[31] A. K. Subramani, "Computations of highly nonlinear free-surface flows, with applications to arbitrary and complex hull forms," Ph.D. dissertation, University of Michigan, Ann Arbor, MI, Oct. 2000.

[32] D. C. Wyatt, "Development and assessment of a nonlinear wave prediction methodology for surface vessels," *Journal of Ship Research*, vol. 44, no. 2, pp. 96–107, 2000.

[33] T. Soomere, "Nonlinear ship wake waves as a source of danger to the coastal environment: a review," *Oceanologia*, vol. 48, pp. 185–202, 2006.

[34] M. Rabaud and F. Moisy, "Ship wakes: Kelvin or Mach angle?" *Physical Review Letters*, vol. 110, p. 214503, May 2013.

[35] Vortical Flow Research Laboratory, Apr. 2017. [Online]. Available: http://web.mit.edu/vfrl/www/

[36] C. Li and Y. Liu, "Fully-nonlinear simulation of the hydrodynamics of a floating body in surface waves by a high-order boundary element method," in *ASME 2015 34th International Conference on Ocean, Offshore and Arctic Engineering*, vol. 9. American Society of Mechanical Engineers, May 2015, p. V009T09A001.

[37] Multidisciplinary Simulation, Estimation, and Assimilation Systems Group, Apr. 2017. [Online]. Available: http://mseas.mit.edu/

[38] W. Sun, P. Tsiotras, T. Lolla, D. N. Subramani, and P. F. J. Lermusiaux, "Multiple-pursuer-one-evader pursuit evasion game in dynamic flow fields," *Journal of Guidance, Control and Dynamics*, Apr. 2017.

[39] ——, "Pursuit-evasion games in dynamic flow fields via reachability set analysis," in *American Control Conference*, 2017, in press.

[40] B. Reed and F. Hover, "Oceanographic pursuit: Networked control of multiple vehicles tracking dynamic ocean features," *Methods in Oceanography*, vol. 10, pp. 21–43, Sep. 2014, special Issue: Autonomous Marine Vehicles.

[41] B. Reed, J. Leighton, M. Stojanovic, and F. Hover, "Multi-vehicle dynamic pursuit using underwater acoustics," in *Robotics Research: The 16th International Symposium ISRR*, ser. Springer Tracts in Advanced Robotics, M. Inaba and P. Corke, Eds., vol. 114. Springer, 2016, pp. 79–94.

[42] T. Lolla, P. J. Haley, Jr., and P. F. J. Lermusiaux, "Path planning in multiscale ocean flows: coordination and dynamic obstacles," *Ocean Modelling*, vol. 94, pp. 46–66, 2015.

[43] D. N. Subramani, T. Lolla, P. J. Haley, Jr., and P. F. J. Lermusiaux, "A stochastic optimization method for energy-based path planning," in *DyDESS 2014*, ser. LNCS, S. Ravela and A. Sandu, Eds., vol. 8964. Springer, 2015, pp. 1–12.

[44] D. N. Subramani and P. F. J. Lermusiaux, "Energy-optimal path planning by stochastic dynamically orthogonal level-set optimization," *Ocean Modeling*, vol. 100, pp. 57–77, 2016.

[45] D. N. Subramani, P. J. Haley, Jr., and P. F. J. Lermusiaux, "Energy-optimal path planning in the coastal ocean," *Journal of Geophysical Research: Oceans*, 2017, in press.

[46] D. N. Subramani, P. F. J. Lermusiaux, P. J. Haley, Jr., C. Mirabito, S. Jana, C. S. Kulkarni, A. Girard, D. Wickman, J. Edwards, and J. Smith, "Time-optimal path planning: Real-time sea exercises," in *Oceans '17 MTS/IEEE Conference*, Aberdeen, Jun. 2017, in press.

[47] J. Edwards, J. Smith, A. Girard, D. Wickman, D. N. Subramani, C. S. Kulkarni, P. J. Haley, Jr., C. Mirabito, S. Jana, and P. F. J. Lermusiaux, "Data-driven learning and modeling of AUV operational characteristics for optimal path planning," in *Oceans '17 MTS/IEEE Conference*, Aberdeen, Jun. 2017, in press.